Molecular and Electronic Structure of a Mixed-Spin Diiron "Wedged" Metallacarborane, $[(CH_3)_2C_2B_4H_4]_2(Fe^{II}(low\ spin))(Fe^{II}(high\ spin))L_2$ [L_2 = 2THF or $(OCH_3)_2C_2H_4$], an Oxidative Fusion Intermediate[1]

Russell N. Grimes,*[2a] Richard B. Maynard,[2a] Ekk Sinn,[2a] Greg A. Brewer,[2a] and Gary J. Long[2b]

Contribution from the Department of Chemistry, University of Virginia, Charlottesville, Virginia 22901, and the Department of Chemistry, University of Missouri—Rolla, Rolla, Missouri 65401. *Received March 29, 1982*

Abstract: An X-ray diffraction study of the purple paramagnetic title compound established it as a dimetallic complex having one iron atom sandwiched between two $(CH_3)_2C_2B_4H_4^{2-}$ ligands (as in the previously characterized red diamagnetic monoiron compound $[(CH_3)_2C_2B_4H_4]_2FeH_2$) with the second iron in a wedging location, coordinated to the complex via four Fe–B interactions. The "outer" iron atom is also bound to a 1,2-dimethoxyethane solvent ligand. The Fe–Fe distance of 2.414 (4) Å is well within bonding range, but the existence of a direct iron–iron bond is in doubt. From magnetic susceptibility and Mössbauer measurements, both iron atoms are assigned 2+ oxidation states with one metal in a low-spin (diamagnetic) configuration and the other high-spin with four unpaired electrons. Comparison with the red monoiron species, from which the diiron complex is prepared by insertion of Fe^{2+}, suggests that the paramagnetism arises from the outer iron atom. The bis(tetrahydrofuran) analogue of the title compound, $[(CH_3)_2C_2B_4H_4]_2Fe_2(THF)_2$, is an intermediate in the conversion of $[(CH_3)_2C_2B_4H_4]_2FeH_2$ to $(CH_3)_4C_4B_8H_8$ via oxidative fusion, as described in the preceding article.

Metal ions can bind to borane and carborane ligands in a remarkable variety of ways.[3] While the earliest metallacarboranes were structural analogues of metallocenes,[4] subsequent work has produced a wealth of structurally diverse species that have few counterparts outside of boron cluster chemistry. One such class consists of the so-called "wedged" complexes, in which the wedging atom occupies a crevice between two carborane ligands (Figure 1). Prior to this work the only structurally established example was the iron–cobalt species[5] in Figure 1a; two other members of this group, based on NMR characterization,[6] are $[(CH_3)_2C_2B_4H_4]_2FeGe$ and its tin analogue (Figure 1b).

This paper describes a detailed study of a new wedge-type complex that exhibits some structurally and electronically unusual features and in addition plays a synthetically significant role: it is an intermediate in the conversion of the monoiron complex $[(CH_3)_2C_2B_4H_4]_2FeH_2$ (Figure 2) to $(CH_3)_4C_4B_8H_8$ via oxidative ligand fusion.[7]

Results and Discussion

The deep red diamagnetic dicarboranyliron(II) complex[8] $[2,3\text{-}(CH_3)_2C_2B_4H_4]FeH_2$ (**1**), on standing in THF solution slowly converts to a deep purple paramagnetic complex as described elsewhere;[7] the same purple compound forms rapidly in the presence of traces of $FeCl_3$. Evaporation of the solvent yields an almost black crystalline material (**2A**), which is extremely air-sensitive but can be purified by recrystallization from THF/hexane under a rigorously O_2-free atmosphere. Although **2A** is obtainable in good yield and in gram quantities, its characterization proved difficult owing to its paramagnetism (which rendered NMR spectra useless) and its decomposition in the mass spectrometer, which precluded observation of a parent molecular ion (only the spectrum of its carborane oxidation product, $(CH_3)_4C_4B_8H_8$, can be seen). The analogous complex (**3A**) obtained from the bis(diethylcarborane) complex $[2,3\text{-}(C_2H_5)_2C_2B_4H_4]_2FeH_2$ exhibits similar properties.

Table I. Positional Parameters and Their Estimated Standard Deviations for $[(CH_3)_2C_2B_4H_4]_2Fe_2(OCH_3)_2C_2H_4$

atom	x	y	z
Fe(1)	0.1100 (6)	0.1349 (3)	0.1760 (5)
Fe(2)	0.2315 (6)	0.0802 (3)	0.3844 (5)
O(1)	0.400 (2)	0.085 (1)	0.593 (2)
O(2)	0.232 (2)	−0.003 (1)	0.465 (2)
C(2)	0.272 (4)	0.187 (2)	0.118 (4)
C(3)	0.182 (4)	0.152 (2)	−0.011 (4)
C(4)	0.180 (4)	−0.056 (2)	0.391 (4)
C(5)	0.349 (4)	−0.018 (2)	0.597 (4)
C(6)	0.362 (4)	0.039 (2)	0.675 (3)
C(7)	0.444 (4)	0.142 (2)	0.652 (3)
C(2′)	−0.107 (4)	0.114 (1)	0.136 (3)
C(3′)	−0.089 (3)	0.175 (1)	0.131 (3)
C(M2)	0.311 (4)	0.245 (2)	0.116 (4)
C(M3)	0.118 (4)	0.189 (2)	−0.153 (3)
C(M2′)	−0.215 (3)	0.075 (2)	0.036 (3)
C(M3′)	−0.192 (4)	0.214 (2)	0.014 (4)
B(4)	0.173 (4)	0.090 (2)	0.005 (4)
B(5)	0.282 (5)	0.077 (2)	0.167 (4)
B(6)	0.351 (4)	0.138 (2)	0.231 (4)
B(7)	0.341 (5)	0.123 (2)	0.056 (4)
B(4′)	0.012 (4)	0.203 (2)	0.271 (4)
B(5′)	0.054 (5)	0.148 (2)	0.369 (4)
B(6′)	−0.033 (4)	0.092 (2)	0.294 (4)
B(7′)	−0.142 (4)	0.152 (2)	0.290 (4)
H(4)	0.08 (0)	0.06 (0)	−0.05 (0)
H(5)	0.33 (3)	0.03 (1)	0.23 (3)
H(6)	0.46 (3)	0.16 (1)	0.32 (3)
H(7)	0.44 (3)	0.12 (1)	0.01 (3)
H(4′)	0.04 (3)	0.25 (1)	0.31 (3)
H(5′)	0.11 (3)	0.15 (1)	0.49 (3)
H(6′)	−0.01 (2)	0.04 (1)	0.31 (2)
H(7′)	−0.26 (3)	0.16 (1)	0.33 (3)
H(1C5)	0.31 (3)	−0.06 (1)	0.67 (3)
H(2C5)	0.46 (3)	−0.03 (1)	0.55 (3)
H(1C6)	0.44 (3)	0.03 (1)	0.76 (3)
H(2C6)	0.26 (3)	0.05 (1)	0.71 (3)

(1) Presented in part at the 182nd National Meeting of the American Chemical Society, New York, Aug 1981; INOR-10.
(2) (a) University of Virginia; (b) University of Missouri.
(3) "Metal Interactions with Boron Clusters"; Grimes, R. N., Ed.; Plenum Press: New York, 1982.
(4) Dunks, G. B.; Hawthorne, M. F. In "Boron Hydride Chemistry"; Muetterties, E. L., Ed.; Academic Press: New York, 1975; Chapter 11.
(5) Maxwell, W. M.; Sinn, E.; Grimes, R. N. *J. Am. Chem. Soc.* **1976**, *98*, 3490.
(6) Maxwell, W. M.; Wong, K.-S.; Grimes, R. N. *Inorg. Chem.* **1977**, *16*, 3094.
(7) Maynard, R. B.; Grimes, R. N., preceding paper in this issue.
(8) Maxwell, W. M.; Miller V. R.; Grimes, R. N. *Inorg. Chem.* **1976**, *15*, 1343.

0002-7863/82/1504-5987$01.25/0

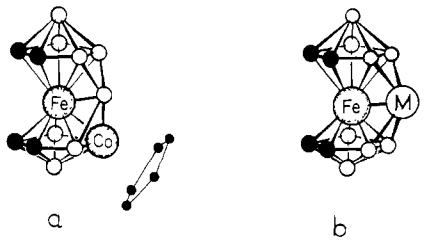

Figure 1. (a) Established structure[5] of $(\eta^5\text{-}C_5H_5)CoFe(CH_3)_4C_4B_8H_8$. (b) Proposed structure[6] of $MFe(CH_3)_4C_4B_8H_8$ (M = Ge or Sn; O = BH; ● = CCH_3).

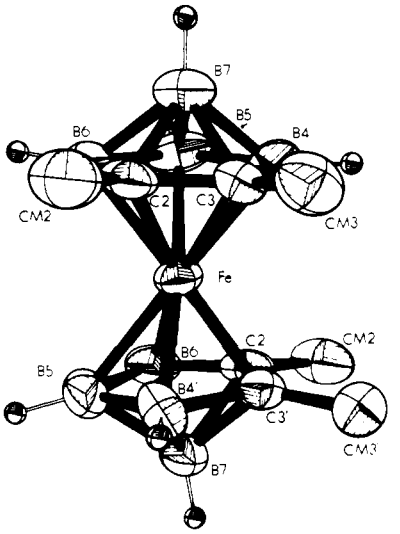

Figure 2. Structure[9] of $[(CH_3)_2C_2B_4H_4]_2FeH_2$ (metal-bound hydrogen atoms not shown).

Despite these difficulties, the nature of the purple species was elucidated from X-ray diffraction, Mössbauer, ESR, and magnetic susceptibility studies. NMR, UV-visible, and infrared data are reported in the accompanying paper.[7]

X-ray Structure Determination. Diffraction data were collected on a crystal grown from a dimethoxyethane (DME) solution of **2A**, under which conditions the pair of THF ligands assumed to be present in **2A** are replaced by a bidentate DME molecule; the DME-solvated complex is labeled **2B**.

The molecular structure and crystal packing of **2B** are depicted in Figures 3 and 4, respectively, while Tables I–III list positional parameters, bond distances, and selected bond angles. The complex consists of two $(CH_3)_2C_2B_4H_4$ carborane units sandwiched around a central iron atom [Fe(1)], with a second iron [Fe(2)] bound to both carborane ligands (via four Fe–B links) and also to DME. The coordination of the two carborane ligands to Fe(1) is similar to that found[9] in the monoiron precursor complex $[(CH_3)_2C_2B_4H_4]_2FeH_2$, (**1**, Figure 2). A comparison of important parameters in these two complexes is as follows (values for the diiron species **2B** are given first): mean Fe–C bond length, 2.062 vs. 2.065 Å; mean Fe–B bond length, 2.132 vs. 2.189 Å; mean C–C (cage) distance, 1.494 vs. 1.484 Å; vector distance from Fe(1) to the C_2B_3 equatorial planes, 1.644 and 1.607 vs. 1.649 Å; dihedral angle between C_2B_3 equatorial planes, 6.56° vs. 7.80°, with the C–CH_3 groups on opposing ligands tilted *toward* each other in both structures. Clearly, the presence of the second metal atom is **2B** does not produce major alterations in the sandwich geometry. There is, however, one signficant difference: the carborane ligands in **2B** are rotated only ~48° from an eclipsed configuration, as opposed to a 90° rotation in **1**.[9] This arrangement evidently allows the outer iron, Fe(2), to bond more efficiently to the two carborane units (see Figure 3) than would be the case in a more nearly staggered configuration such as is found in the monoiron species **1**.

(9) Pipal, J. R.; Grimes, R. N. *Inorg. Chem.* **1979**, *18*, 263.

Table II. Bond Distances (Å) in $[2,3\text{-}(CH_3)_2C_2B_4H_4]_2Fe_2(OCH_3)_2C_2H_4$(2B)

Fe(1)-Fe(2)	2.414 (4)	C(2')-C(M2')	1.524 (24)
Fe(1)-C(2)	2.108 (27)	C(3')-C(M3')	1.585 (24)
Fe(1)-C(3)	2.087 (23)	C(3')-B(4')	1.584 (26)
Fe(1)-B(4)	2.137 (25)	B(4')-B(5')	1.611 (32)
Fe(1)-B(5)	2.113 (31)	B(5')-B(6')	1.583 (32)
Fe(1)-B(6)	2.182 (24)	C(2')-B(6')	1.590 (25)
Fe(1)-C(2')	2.022 (21)	C(2')-B(7')	1.810 (29)
Fe(1)-C(3')	2.031 (20)	C(3')-B(7')	1.785 (28)
Fe(1)-B(4')	2.137 (26)	B(4')-B(7')	1.901 (32)
Fe(1)-B(5')	2.045 (26)	B(5')-B(7')	1.811 (34)
Fe(1)-B(6')	2.175 (26)	B(6')-B(7')	1.732 (32)
C(2)-C(3)	1.557 (27)	Fe(2)-B(5)	2.231 (27)
C(2)-C(M2)	1.418 (29)	Fe(2)-B(6)	2.440 (26)
C(3)-C(M3)	1.604 (25)	Fe(2)-B(5')	2.248 (28)
C(3)-B(4)	1.461 (30)	Fe(2)-B(6')	2.427 (24)
B(4)-B(5)	1.665 (30)	Fe(2)-O(1)	2.234 (12)
B(5)-B(6)	1.616 (38)	Fe(2)-O(2)	2.088 (16)
C(2)-B(6)	1.626 (33)	O(1)-C(6)	1.417 (23)
C(2)-B(7)	1.782 (34)	O(1)-C(7)	1.482 (25)
C(3)-B(7)	1.616 (30)	O(2)-C(4)	1.457 (21)
B(4)-B(7)	1.716 (33)	O(2)-C(5)	1.499 (21)
B(5)-B(7)	1.693 (36)	C(5)-C(6)	1.510 (27)
B(6)-B(7)	1.694 (29)	⟨C-H⟩	1.17
C(2')-C(3')	1.430 (25)	⟨B-H⟩	1.20

Table III. Selected Bond Angles (deg)

Angles on Carborane Equatorial Atoms			
B(6)-C(2)-C(3)	103.3 (20)	B(6')-C(2')-C(3')	109.3 (17)
C(2)-C(3)-B(4)	118.2 (20)	C(2')-C(3')-B(4')	115.4 (18)
C(3)-B(4)-B(5)	103.7 (20)	C(3')-B(4')-B(5')	99.7 (19)
B(4)-B(5)-B(6)	107.4 (21)	B(4')-B(5')-B(6')	111.4 (19)
B(5)-B(6)-C(2)	106.9 (18)	B(5')-B(6')-C(2')	103.2 (18)
C(M2)-C(2)-Fe(1)	139.5 (19)	C(M2')-C(2')-Fe(1)	138.6 (14)
C(M2)-C(2)-C(3)	126.3 (21)	C(M2')-C(2')-C(3')	129.5 (18)
C(M2)-C(2)-B(6)	127.8 (23)	C(M2')-C(2')-B(6')	118.4 (18)
C(M2)-C(2)-B(7)	133.6 (22)	C(M2')-C(2')-B(7')	125.4 (17)
Angles around Fe(1)			
C(2)-Fe(1)-C(3)	43.56 (76)	C(2')-Fe(1)-C(3')	41.31 (70)
C(3)-Fe(1)-B(4)	40.45 (80)	C(3')-Fe(1)-B(4')	44.57 (73)
B(4)-Fe(1)-B(5)	46.14 (85)	B(4')-Fe(1)-B(5')	45.24 (90)
B(5)-Fe(1)-B(6)	44.2 (10)	B(5')-Fe(1)-B(6')	43.92 (88)
B(6)-Fe(1)-C(2)	44.50 (89)	B(6')-Fe(1)-C(2')	44.33 (70)
Angles around Fe(2)			
Fe(1)-Fe(2)-B(5)	53.93 (78)	B(6)-Fe(2)-B(5')	90.56 (99)
Fe(1)-Fe(2)-B(6)	53.41 (55)	B(6)-Fe(2)-B(6')	106.75 (78)
Fe(1)-Fe(2)-B(5')	51.90 (65)	B(6)-Fe(2)-O(1)	100.66 (66)
Fe(1)-Fe(2)-B(6')	53.40 (57)	B(6)-Fe(2)-O(2)	140.72 (82)
Fe(1)-Fe(2)-O(1)	143.90 (49)	B(5')-Fe(2)-B(6')	39.35 (84)
Fe(1)-Fe(2)-O(2)	139.32 (43)	B(5')-Fe(2)-O(1)	112.49 (78)
B(5)-Fe(2)-B(6)	40.17 (97)	B(5')-Fe(2)-O(2)	127.12 (85)
B(5)-Fe(2)-B(5')	105.8 (10)	B(6')-Fe(2)-O(1)	139.20 (66)
B(5)-Fe(2)-B(6')	95.14 (91)	B(6')-Fe(2)-O(2)	98.85 (75)
B(5)-Fe(2)-O(1)	124.88 (80)	O(1)-Fe(2)-O(2)	76.78 (59)
B(5)-Fe(2)-O(2)	109.43 (94)		
Angles in Dimethoxyethane Ligand			
Fe(2)-O(1)-C(6)	103.8 (11)	C(6)-O(1)-C(7)	124.3 (15)
Fe(2)-O(2)-C(5)	118.0 (12)	C(5)-O(2)-C(4)	107.5 (16)
Fe(2)-O(1)-C(7)	116.9 (12)	O(1)-C(6)-C(5)	113.3 (17)
Fe(2)-O(2)-C(4)	129.9 (12)	O(2)-C(5)-C(6)	99.3 (17)

The outer iron atom in **2B** is within normal bonding distance of the central iron [2.414 (4) Å] and of one boron atom on each ligand [**B**(5), 2.231 (27) Å; B(5'), 2.248 (28) Å], but the Fe(2)–B(6) and Fe(2)–**B**(6') links are quite long, exceeding 2.4 Å although still within at least weak bonding range. The nature of the Fe(1)–Fe(2) interaction presents an intriguing problem which is further addressed below.

The DME ligand is coordinated to Fe(2) in normal fashion, and the two oxygen atoms form an essentially coplanar array with Fe(2) and Fe(1) (maximum deviation 0.004 Å; (see table of mean planes in the supplementary material). Overall, the molecule has approximate C_2 symmetry with respect to the Fe(1)–Fe(2) axis. There is no direct or indirect evidence for hydrogen ligands on

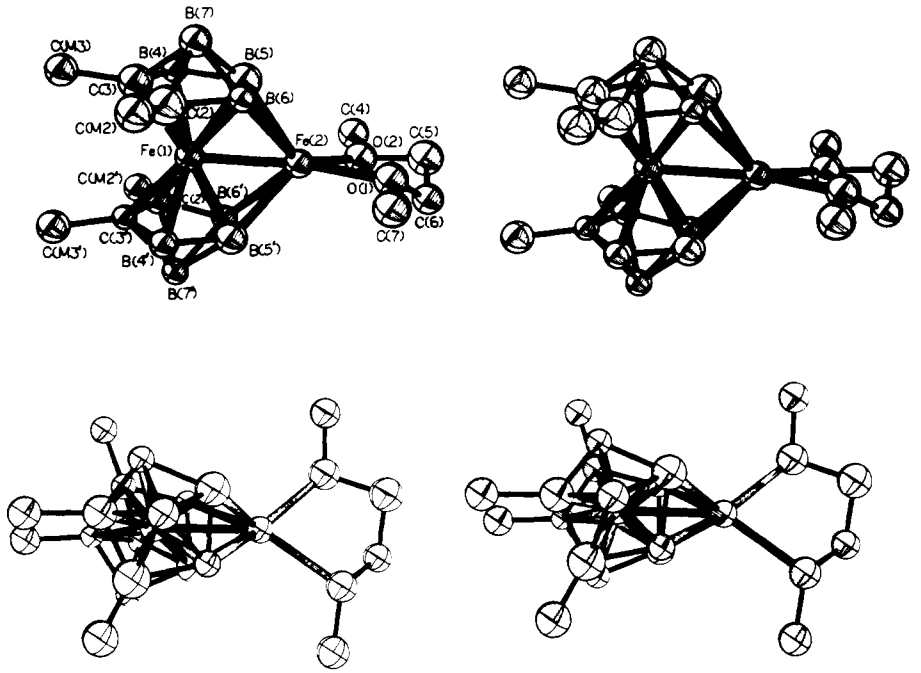

Figure 3. Stereoviews of $[(CH_3)_2C_2B_4H_4]_2Fe_2(OCH_3)_2C_2H_4$ from the side (top) and approximately along the B(7)–Fe(1)–B(7′) axis (bottom).

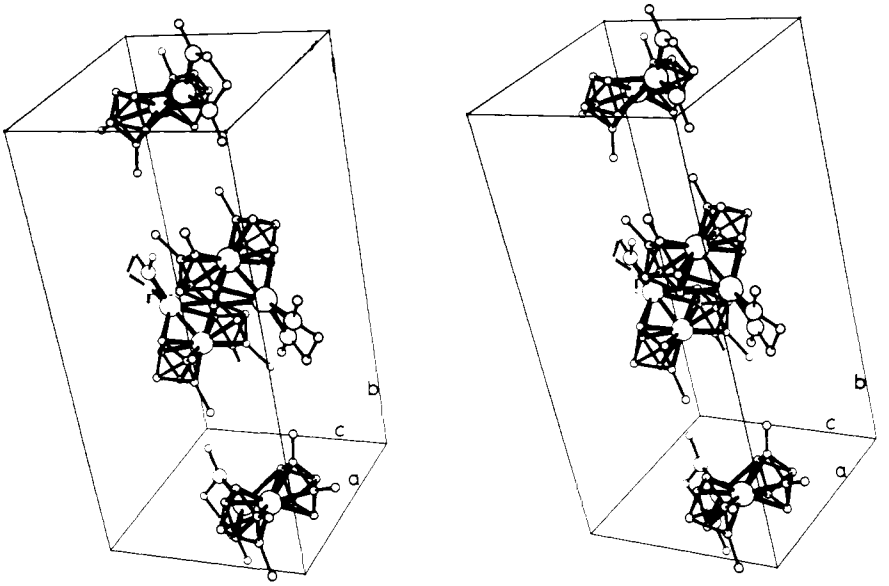

Figure 4. Unit cell packing.

either metal atom, in contrast to the monoiron complex **1** where the two metal-bound hydrogens were observed both in the proton NMR spectrum[8] and, indirectly, from the tilt of the carborane ligands as revealed in the X-ray diffraction study.[9] In the diiron species, the ligand tilt is dictated by the coordination to Fe(2). Even if hydrogen ligands were present, they probably could not be detected from the available X-ray data, but other evidence argues against their presence, as will be shown.

The structure of **2B** roughly resembles that of the iron–cobalt complex $[(CH_3)_2C_2B_4H_4]_2FeCo(C_5H_5)$ (Figure 1a), except that in that compound the inserted cobalt atom has displaced a BH unit which is forced into a wedging position,[5] whereas in **2B** the metal itself occupies the wedge. These two complexes and their $[(CH_3)_2C_2B_4H_4]_2FeM$ (M = Ge, Sn) relatives[6] were all prepared by introduction of a metal–ligand unit into $[(CH_3)_2C_2B_4H_4]_2FeH_2$ with net displacement of the hydrogen ligands; it appears that wedge-type complexes may in fact form a potentially large family of metallacarboranes, perhaps even involving other ligands such as dicarbollide ($C_2B_9H_{11}^{2-}$). Indeed, evidence for the existence of $(C_2B_9H_{11})_2Ni_2$, which could well have a wedged structure, has been reported.[10]

Mössbauer Data. The spectra of **2B** at 78 and 4.2 K are virtually identical. Figure 5 presents the spectra of **2B** and of its precursor **1**, for comparison; data for these two compounds, as well as for $[(CH_3)_2C_2B_4H_4]_2Fe_2(THF)_2$ (**2A**), $[(C_2H_5)_2C_2B_4H_4]_2Fe_2(THF)_2$ (**3A**), several other ferracarboranes, and some related iron complexes, are listed in Table IV. The spectra of **2A**, **2B**, and **3A** all exhibit four-line patterns that clearly indicate the presence of two iron atoms. In the absence of other information, further interpretation of these spectra would be ambiguous; typical Mössbauer isomer shifts observed elsewhere for the various oxidation and spin states of iron would not necessarily be applicable to these unusual structures.[11] However, from magnetic and ESR evidence (vide infra), the two iron atoms in the diiron complexes are assigned oxidation states of low-spin Fe(II) and high-spin Fe(II), respectively. Moreover, the spectra of **2A** and **3A**, in which the second and fourth lines (reading left to right) are distinctly

(10) Borodinsky, L. Ph.D. Thesis, University of Virginia, Charlottesville, VA, 1982; pp 165–166.

(11) Mössbauer spectra have previously been recorded for several iron complexes of the dicarbollide ($C_2B_9H_{11}^{2-}$) ligand, cited in Table IV.

Table IV. Mössbauer Spectral Data[a]

compound	T, K	ΔE_Q	δ	Γ_1	Γ_2	A, %	assignment
$[(CH_3)_2C_2B_4H_4]_2FeH_2$ (1)	78	2.25	0.37	0.25	0.25	100	LS Fe(II)
	4.2	2.25	0.37	0.30	0.30	100	LS Fe(II)
$[(CH_3)_2C_2B_4H_4]_2Fe_2\cdot 2THF$ (2A)	78	1.91	0.31	0.27	0.35	75	LS Fe(II)
		1.82	0.98	0.34	0.29	25	HS Fe(II)
$[(C_2H_5)_2C_2B_4H_4]_2Fe_2\cdot 2THF$ (3A)	78	1.78	0.29	0.25	0.30	50	LS Fe(II)
		1.87	0.95	0.34	0.30	50	HS Fe(II)
$[(CH_3)_2C_2B_4H_4]_2Fe_2\cdot DME$ (2B)	78	1.84	0.29	0.28	0.27	53	LS Fe(II)
		1.86	0.98	0.28	0.29	47	HS Fe(II)
	4.2	1.86	0.30	0.31	0.32	54	LS Fe(II)
		1.86	0.99	0.31	0.30	46	HS Fe(II)
$(C_8H_{10})Fe[(CH_3)_2C_2B_4H_4]$[b]	78	1.05	0.35	0.29	0.29	90	LS Fe(II)
$[(CH_3)_4N][Fe^{III}(C_2B_9H_{11})_2]$[c]	80	0.64	0.26	0.73	0.62	100	HS Fe(III)
$[(CH_3)_4N]_2[Fe^{II}(C_2B_9H_{11})_2]$[c]	80	2.80	0.32	0.27	0.27	100	LS Fe(II)
$(C_5H_5)Fe^{III}(C_2B_9H_{11})$[d]	140	0.53	0.37			100	LS Fe(III)
$(C_5H_5)_2Fe^{II}$[d]	78	2.40	0.55	0.25	0.25	100	LS Fe(II)

[a] Data are given in millimeters per second relative to α-iron foil at room temperature. [b] Synthesis and structure: Maynard, R. B.; Grimes, R. N., 182nd National Meeting of the American Chemical Society, New York, Aug 1981; INOR-11. [c] Birchall, T.; Drummond, I. *Inorg. Chem.* 1971, *10*, 399. [d] Herber, R. H. *Ibid.* 1969, *8*, 174.

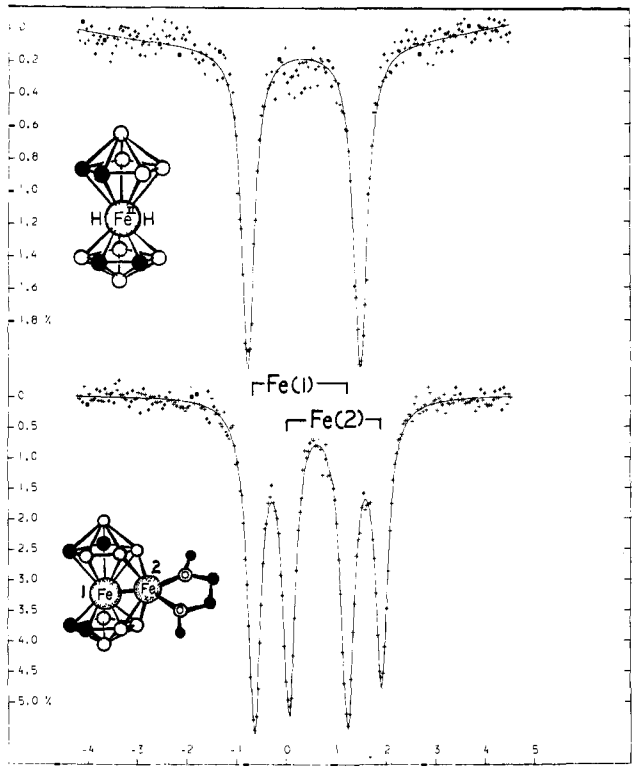

Figure 5. Mössbauer spectra of $[(CH_3)_2C_2B_4H_4]_2FeH_2$ (**1**) (top) and $[(CH_3)_2C_2B_4H_4]_2Fe_2(OCH_3)_2C_2H_4$ (**2B**) (bottom), taken at 4.2 K.

weaker than the others permits assignment of the two doublets as shown in Figure 5.

This interpretation is consistent with the observed molecular structure of **2B** depicted in Figure 3. Thus, the Mössbauer parameters of the central iron [Fe(1)] are typical for low-spin iron(II) (see Table IV), whereas the isomer shifts observed for the outer iron [Fe(2)] (0.94–0.99 mm/s) are intermediate between the values normally observed for Fe(II) in octahedral vs. tetrahedral environments. This suggests a quasi-tetrahedral description for the Fe(2) coordination, which can be envisioned if Fe(2) is considered to bond primarily to O(1), O(2), and the midpoints of the B(5)–B(6) and B(5′)–B(6′) edges, with little, if any, direct Fe–Fe binding (see below). Further, the observation that the peak areas for Fe(1) appear slightly larger than those for Fe(2) (see Figure 5) is consistent with the presumption that the low-spin metal [Fe(1)] is more tightly bound into the molecule than is the high-spin metal [Fe(2)], resulting in a higher recoil-free fraction for the former.

Table V. Magnetic Moments (μ, in μ_B) for $[(CH_3)_2C_2B_4H_4]_2Fe_2(OCH_3)_2C_2H_4$

T, K	μ	T, K	μ	T, K	μ
4.50	4.708	16.7	4.909	57.5	5.178
5.21	4.734	19.8	4.935	65.3	5.138
5.67	4.734	22.4	4.965	72.7	5.179
6.14	4.758	24.5	4.954	78.0	5.175
7.16	4.770	26.3	4.989	86.5	5.215
8.32	4.808	34.5	5.089	94.3	5.259
9.89	4.841	41.6	5.143	101.4	5.282
11.64	4.864	49.1	5.104	108.5	5.303
14.80	4.928				

The Mössbauer spectra of **2A** and **3A** are virtually identical, showing that replacement of CH_3 by C_2H_5 groups on the carboranyl carbon atoms has little effect on the electronic environment of the metal atoms. One might, however, expect replacement of THF ligands on Fe(2) by DME to produce a measurable effect on that iron atom, but aside from the weak intensity of the Fe(2) lines, which is probably caused in part by sample degradation, the spectrum of **2A** is quite similar to that of the corresponding DME complex **2B**.

Magnetic Susceptibility and Electron Spin Resonance. The molar susceptibility of **2B** was measured as a function of temperature between 4.50 and 108.50 K (Table V), over which range the magnetic moment μ (corrected for θ) rises from 4.7 to 5.3 μ_B. These data are consistent with a model (i) containing both high-spin and low-spin Fe(II); only the high-spin iron, with four unpaired electrons, contributes significantly to the observed moment, and there is essentially no magnetic coupling between the metal centers. On this basis we can formulate **2B** as $[(CH_3)_2C_2B_4H_4]_2Fe^{II}{}_{LS}Fe^{II}{}_{HS}(OCH_3)_2C_2H_4$, where the low-spin iron occupies the central site [Fe(1) in Figure 3] analogous to its counterpart in the monoiron precursor $[(CH_3)_2C_2B_4H_4]_2Fe^{II}{}_{LS}H_2$; the high-spin iron is then in the outer (wedging) location, Fe(2).

An alternative model (ii) which was considered,[1] has both metal atoms in the 3+ oxidation state, in turn requiring the presence of two formal H^- ligands to provide charge balance. In that case the formula would be $[(CH_3)_2C_2B_4H_4]_2Fe^{III}{}_{LS}Fe^{III}{}_{HS}(H)_2(OCH_3)_2C_2H_4$. Conceivably, if the two iron atoms were antiferromagnetically coupled to just the right magnitude, four unpaired electrons would be observed, and the magnetic susceptibility data would be compatible with this second model. This possibility, considered rather unlikely in any event, is rendered even more improbable by the behavior of the magnetic moment μ at low temperature; for model ii, theory[12] predicts that μ should level

(12) The "spin-only" values of μ for $Fe^{III}{}_{HS}$ and $Fe^{III}{}_{LS}$ would be $\sqrt{35}$ and $\sqrt{3}$ μ_B, respectively, averaging to $\sqrt{38} \simeq 6.16$ μ_B. However, low-spin iron(III) complexes typically exhibit spin–orbit coupling that produces a higher moment than the "spin-only" value; in this case one would predict an average value of perhaps 6.3 μ_B at the upper temperature limit.

off at ~4.90 μ_B with decreasing temperature, clearly inconsistent with the observed data.

Further strong, if not conclusive, support for model i in preference to ii is given by ESR experiments conducted at −160 °C and at room temperature. At the lower temperature the spectrum consists of one signal at $g = 2.035$, while at room temperature no spectrum is observed. These data are compatible with a single paramagnetic center and represent typical behavior for Fe(II) high-spin complexes, but would be very difficult to reconcile with the presence of Fe(III) as in model ii. Hence, while not totally ruling out other possibilities, we regard model i, as presented above, as almost certainly correct. It is moreover quite reasonable in light of the synthesis of the diiron species via reaction of diamgnetic $(R_2C_2B_4H_4)_2Fe^{II}H_2$ with $FeCl_3$ as described in the preceding paper;[7] one can readily visualize replacement of the iron-bound protons in the monoiron complex by an FeL_2^{2+} unit (L_2 = DME or 2THF), with the second iron retaining its high-spin, weak-field electronic structure. This is, of course, quite consistent with the Mössbauer evidence for quasi-tetrahedral coordination of Fe(2) as discussed above. Such a description, however, ignores the Fe(1)–Fe(2) interaction, which deserves further comment.

Metal–Metal Bonding in $(R_2C_2B_4H_4)_2Fe_2{\cdot}L_2$ Complexes. The iron–iron distance in **2B** [2.414 (4) Å] is well within normal bonding range, compared, for example, to Fe–Fe separations of 2.52 Å in metallic iron[13] and 2.591 (5) Å in $(1,2\text{-}C_2B_9H_{11})_2Fe_2(CO)_4$,[14] in which both iron atoms are in a ferracarborane framework and are linked to each other via a doubly carbonyl-bridged Fe–Fe single bond (the analogous cyclopentadienyl species, *cis*- and *trans*-$[(\eta^5\text{-}C_5H_5)Fe(CO)_2]_2$, have iron–iron distances of 2.533 (6)[15] and 2.534 (6) Å,[16] respectively). On the basis of the short metal–metal separation in **2B**, the Fe–Fe vector is represented as bonding in Figure 3. Nevertheless, it is not certain that significant bonding electron density is present between Fe(1) and Fe(2). The magnetic and ESR evidence discussed above indicates that the two metal centers are magnetically independent. Undoubtedly, at least indirect electronic interaction exists between the metals, given that Fe(1) resides in an electron-delocalized metallacarborane matrix to which Fe(2) is clearly bonded, but the question of a direct iron–iron bond is another matter. If the Fe–Fe interaction is considered as bridged by the two B–B edges to which both metals are mutually linked, the situation may resemble B_2H_6, in which it has been calculated that direct boron–boron bonding is negligible and nearly all the interboron electron density is located in the B–H–B bridges.[17] Further insight into this problem must await future studies, which we hope will include new wedge-type complexes with other metals in a variety of spin states.

Experimental Section

All reactions were carried out in a dry nitrogen atmosphere in Schlenk ware, glovebox, or high-vacuum apparatus.

Materials. 2,3-Dimethyl-2,3-dicarbahexaborane(8), $(CH_3)_2C_2B_4H_6$, was prepared from B_5H_9, $(CH_3)_2C_2$, and $(CH_3)_3N$ as described elsewhere.[18] Anhydrous ferrous chloride (alfa) was dried at high temperature in vacuo prior to use. Tetrahydrofuron (THF) and 1,2-dimethoxyethane (DME) were dried by reflux over sodium benzophenone ketyl, and hexane was dried by reflux over calcium hydride. Sodium hydride (50% in mineral oil, Alfa) was washed with pentane prior to use. Silica gel 60 (Merck) was prepared for inert atmosphere use via the method suggested by Shriver.[19]

Instrumentation. Magnetic susceptibilities were measured on a Squid magnetometer from 4 to 108 K. The calibration of the instrument and techniques of measurement were as described previously.[20,21] Electron spin resonance (ESR) spectra were recorded on a Varian E-109 spectrometer at 9.1 GHz. The cavity temperature was maintained with a Varian variable temperature controller using liquid nitrogen as the carrier gas. The sample was held in a quartz tube that had been presealed in an atmosphere of dry N_2. ^{57}Fe Mössbauer spectra were obtained in an inert atmosphere on Ranger or Harwell constant-acceleration spectrometers that utilized room-temperature rhodium-matrix sources and were calibrated with natural α-iron foil. The powdered samples were mixed with petroleum jelly to provide an absorber with a random polycrystalline orientation and thickness of ca. 7 (mg of Fe)/cm^2. The Mössbauer effect parameters reported herein have error limits of ±0.002 mm/s.

Preparation of $[(CH_3)_2C_4B_4H_2]_2Fe_2{\cdot}2THF$ (2A). A solution of $Na^+[(CH_3)_2C_2B_4H_5]^-$ in THF was prepared by adding, via a sidearm tipper, 2.01 g (19.3 mmol) of $(CH_3)_2C_2B_4H_6$ onto 0.68 g (28 mmol) of NaH in 30 mL of THF. This solution was filtered in vacuo onto 1.41 g (11.0 mmol) of anhydrous $FeCl_2$ in a 100-mL Schlenk tube cooled in liquid nitrogen. The solution was allowed to warm to ~−20 °C and stirred at that temperature until it acquired a deep red color. Subsequently it was allowed to warm to room temperature and stirred overnight, during which the color changed to dark purple. The THF was removed in vacuo, and the Schlenk tube was transferred into the glovebox, where the nearly black material was placed on a 2-cm layer of silica gel on a sintered glass filter and washed with hexane to remove any unreacted red $[(CH_3)_2C_2B_4H_4]_2FeH_2$. The material remaining on the silica gel was washed through with THF and the THF removed in vacuo. The dark colored residue was recrystallized from a 4:1 hexane/THF solution to give 1.47 g of $[(CH_3)_2C_2B_4H_4]_2Fe_2{\cdot}2THF$ (58% yield based on total iron required).

Conversion of $[(CH_3)_2C_2B_4H_4]_2Fe_2{\cdot}2THF$ (2A) to $[(CH_3)_2C_2B_4H_4]_2Fe_2{\cdot}DME$ (2B). A 0.50-g sample of **2A** was placed in 30 mL of 1,2-DME and stirred at room temperature for 1 h. The solvent was removed in vacuo and the residue recrystallized from a 4:1 hexane:DME solution to give an essentially quantitative yield of dark purple $[(CH_3)_2C_2B_4H_4]_2Fe_2{\cdot}DME$ (2B).

X-ray Structure Determination on $[(CH_3)_2C_2B_4H_4]_2Fe_2{\cdot}DME$. Although **2A** and **2B** crystallized readily, it proved difficult to obtain diffraction-quality crystals. Ultimately, acceptable crystals were obtained by dissolving **2B** in a minimum volume of DME in a 50-mL Schlenk tube and carefully layering a large excess of hexane on top. The apparatus was placed in an insulated bath containing ethylene glycol, covered with aluminum foil, and placed in a freezer at ~−1.5 °C for 2 days, during which dark purple-black crystals of **2B** formed. Several crystals were mounted with Corning high-vacuum stopcock grease in thin-walled glass capillaries under nitrogen, and following examination by preliminary precession photographs, one thin crystal was selected for data collection. Crystal data were as follows: $Fe_2C_{12}B_8O_2H_{30}$; M_r 404.6; space group $P2_1/n$; $Z = 4$; $a = 9.320$ (7) Å, $b = 23.39$ (2) Å, $c = 9.546$ (5) Å; $\beta = 103.53$ (5)°; $V = 2023$ Å^3; μ (Mo Kα) = 147 cm^{-1}; $\rho_{calcd} = 1.328$ g cm^{-3}. Crystal dimensions could not be measured owing to the capillary mounting. The procedures followed in data collection and processing have been described elsewhere.[22] The values of the parameters A and B, used in the calculation of scan widths,[22] were 0.60 and 0.35, and range of 2θ was 1.5–46°. The intensities of three standard reflections, monitored at regular intervals, showed no greater fluctuations during data collection than would be expected from Poisson statistics. The raw intensity data were corrected for Lorentz–polarization effects, but the irregularity of crystal shape and the capillary mounting prevented correction for absorption. A total of 1751 reflections was measured, of which 955 had $F_o^2 > 2\sigma(F_o)^2$, where F_o^2 was measured from counting statistics ($p = 0.03$).[23] Only the latter data were used in the final refinement of structural parameters.

Solution and Refinement of the Structure. Full-matrix least-squares refinement was based on F, and the function minimized was $w(|F_o| - |F_c|)^2$. The weights w were taken as $[2F_o/\sigma(F_o^2)]^2$, where $|F_o|$ and $|F_c|$ are the observed and calculated structure factor amplitudes. The atomic scattering factors for non-hydrogen atoms were taken from Cromer and Waber[24] and those for hydrogen from Stewart et al.[25] The effects of

(13) Wells, A. F. "Structural Inorganic Chemistry", 4th ed.; Clarendon Press: Oxford, 1975; p 1022.
(14) Greene, P. T.; Bryan, R. F. *Inorg. Chem.* **1970**, *9*, 1464.
(15) Bryan, R. F.; Greene, P. T.; Newlands, M. J.; Field, D. S. *J. Chem. Soc. A* **1970**, 3068.
(16) Bryan, R. F.; Greene, P. T. *J. Chem. Soc. A* **1970**, 3064.
(17) (a) Lipscomb, W. N. *Acc. Chem. Res.* **1973**, *6*, 257. (b) Buenker, R. J.; Peyerimhoff, S. D.; Allen, L. C.; Whitten, J. L. *J. Chem Phys.* **1966**, *45*, 2835.
(18) Hosmane, N. S.; Grimes, R. N. *Inorg. Chem.* **1979**, *18*, 3294.
(19) Shriver, D. F. "The Manipulation of Air-Sensitive Compounds"; McGraw-Hill: New York, 1969; p 152.
(20) O'Connor, C. J.; Sinn, E.; Cukauskas, E. J.; Deaver, B. S., Jr. *Inorg. Chim. Acta* **1979**, *32*, 29.
(21) O'Connor, C. J.; Deaver, B. S., Jr.; Sinn, E. *J. Chem. Phys.* **1979**, *70*, 5161.
(22) Finster, D. C.; Sinn, E.; Grimes, R. N. *J. Am. Chem. Soc.* **1981**, *103*, 1399.
(23) Corfield, P. W. R.; Doedens, R. J.; Ibers, J. A. *Inorg. Chem.* **1967**, *6*, 197.
(24) Cromer, D. T.; Waber, J. T. "International Tables for X-ray Crystallography"; Kynoch Press: Birmingham, England; Vol. IV, 1974.
(25) Stewart, R. F.; Davidson, E. R.; Simpson, W. T. *J. Chem. Phys.* **1965**, *42*, 3175.

anomolous dispersion for all non-hydrogen atoms were included in F by using the values of Cromer and Ibers[26] for $\Delta f'$ and $\Delta f''$.

The positions of the iron atoms were established from a three-dimensional Patterson function calculated from all the intensity data, and the remaining non-hydrogen atoms were located from successive Fourier difference maps. The positions of several hydrogen atoms were calculated; these values were included in the refinement for a few cycles and thereafter held fixed. Anisotropic thermal parameters were introduced for the two iron atoms, but the remaining atoms were refined isotropically. The error in an observation of unit weight was 2.71, and the largest parameter shift in the final cycle of refinement was 0.08 times the estimated standard deviation.

The model converged with $R = 0.112$ and $R_w = 0.112$, where $R = \sum||F_o| - |F_c||/\sum|F_o|$ and $R_w = (\sum w(|F_o| - |F_c|)^2/\sum w|F_o|^2)^{1/2}$. Tables of observed and calculated structure factors, positional and thermal parameters, and mean planes are available (see supplementary material paragraph). The computer system and programs are described elsewhere.[27]

Acknowledgment. This work was supported in part by the National Science Foundation, Grant No. CHE 79-09948.

Registry No. 1, 83096-03-1; **2A**, 83159-76-6; **2B**, 83159-77-7; $N_9[(CH_3)_2C_2B_4H_5]$, 54244-93-8; $FeCl_2$, 7758-94-3.

Supplementary Material Available: Tables of calculated and observed structure factors, positional and thermal parameters, and calculated least-squares planes (9 pages). Ordering information is given on any current masthead page.

(26) Cromer, D. T.; Ibers, J. A., in ref 24.

(27) Freyberg, D. P.; Mockler, G. M.; Sinn, E. *J. Chem. Soc., Dalton Trans.* **1976**, 447.

Oxygenation Patterns for Substituted *meso*-Tetraphenylporphyrin Complexes of Iron(II). Spectroscopic Detection of Dioxygen Complexes in the Absence of Amines

Lechoslaw Latos-Grazynski, Ru-Jen Cheng, Gerd N. La Mar, and Alan L. Balch*

Contribution from the Department of Chemistry, University of California, Davis, California 95616. *Received January 22, 1982*

Abstract: The reaction of dioxygen with iron(II) porphyrins in inert solvents has been studied by ^1H NMR spectroscopy in order to detect the presence of reactive intermediates. Sterically hindered porphyrins have been examined in which the formation of peroxo- and oxo-bridged dimeric structure is limited. The iron(II) porphyrins studied have ^1H NMR spectra characteristic of intermediate-spin ($S = 1$), four-coordinate species. Reduction of [*meso*-tetrakis(2,4,6-trimethoxyphenyl)porphyrin]iron(III) chloride ($[T(2,4,6\text{-}MeO)_3PP]Fe^{III}Cl$) or [*meso*-tetrakis(2,4,6-triethoxyphenyl)porphyrin]iron(III) chloride ($[T(2,4,6\text{-}EtO)_3PP]Fe^{III}Cl$) with either aqueous sodium dithionite or zinc amalgam in dichloromethane solution produces $[T(2,4,6\text{-}MeO)_3PP]Fe^{II}$ or $[T(2,4,6\text{-}EtO)_3PP]Fe^{II}$. The previously reported reduction of these two porphyrins with piperidine has been reexamined and shown to form the bis(piperidine) adducts of the iron(II) porphyrins. Addition of dioxygen to paramagnetic [*meso*-tetrakis($\alpha,\alpha,\alpha,\alpha$-*o*-pivalamidophenyl)porphyrin]iron(II) ($[TpivPP]Fe^{II}$) in toluene solution below −70 °C produces a new diamagnetic complex that is formulated as $[TpivPP]FeO_2$. ^1H NMR spectroscopic observations indicated that, on warming, this species is successively converted to $[TpivPP]Fe^{III}O_2Fe^{III}[TpivPP]$ and to $[TpivPP]Fe^{III}OFe^{III}[TpivPP]$. The latter has been previously isolated. Reaction of $[TpivPP]FeO_2$ with *N*-methylimidazole (*N*-MeIm) at −70 °C results in the formation of (*N*-MeIm)$[TpivPF]FeO_2$. Addition of dioxygen to $[T(3,4,5\text{-}MeO)_3PP]Fe^{II}$ at −70 °C in toluene solution results in the formation of diamagnetic $[T(3,4,5\text{-}MeO)_3PP]FeO_2$. This, on warming, is converted to $[T(3,4,5\text{-}MeO)_3PP]FeO_2Fe[T(3,4,5\text{-}MeO)_3PP]$ and then to $[T(3,4,5\text{-}MeO)_3PP]FeOH$ and $[T(3,4,5\text{-}MeO)_3PP]FeOFe[T(3,4,5\text{-}MeO)_3PP]$ as the final stable products. Addition of dioxygen to $[T(2,4,6\text{-}MeO)_3PP]Fe^{II}$ and $[T(2,4,6\text{-}EtO)_3PP]Fe^{II}$ in dichloromethane solution at −70 °C produces diamagnetic dioxygen adducts. On warming, these undergo dissociation to form the parent iron(II) complex and irreversible oxidation to form iron(III) porphyrin hydroxide and chloride.

The reactions of dioxygen with iron(II) porphyrins have been intensively studied.[1-5] The conditions necessary to obtain reversible coordination of dioxygen, rather than irreversible oxidation to produce iron(III) porphyrins, have received particular attention. The extraordinary attention given to reversible coordination arises because reversible binding is required for the operation of the dioxygen transport and storage proteins, hemoglobin and myoglobin.[6] In synthetic systems, reversible dioxygen binding involves a ligand exchange reaction (eq 1) in which dioxygen replaces another axial ligand. Usually the axial ligand is a heterocyclic

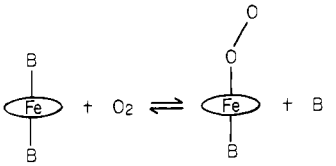

(1)

amine, pyridine, or *N*-methylimidazole.

In the absence of an axial base, PFe^{II}[7] reacts with dioxygen to produce the antiferromagnetic μ-oxo dimer PFeOFeP as the ultimate product. The probable pathway leading to this product is shown in eq 2. We have undertaken examination of this process utilizing high-field ^1H NMR spectroscopy to detect the iron

(1) James, B. R. "The Porphyrins"; Dolphin, D., Ed.; Academic Press: New York, 1978; Vol. 5, pp 205-302.
(2) Jones, P. D.; Summerville, D. A.; Basolo, F. *Chem. Rev.* **1979**, *79*, 139-178.
(3) Collman, J. P. *Acc. Chem. Res.* **1977**, *10*, 265-272.
(4) Collman, J. P.; Halpert, T. R.; Suslick, K. S. In "Metal Ion Activation of Dioxygen"; Spiro, T. G., Ed.; Wiley: New York, 1980; pp 1-72.
(5) Traylor, T. G. *Acc. Chem. Res.* **1981**, *14*, 102-109.
(6) Perutz, M. F. *Annu. Rev. Biochem.* **1979**, *48*, 327-386.

(7) Abbreviations used are: P, porphyrin dianions; H_2[TpivPP], *meso*-tetrakis($\alpha,\alpha,\alpha,\alpha$-*o*-pivalamidophenyl)porphyrin; $H_2[T(2,4,6\text{-}MeO)_3PP]$, *meso*-tetrakis(2,4,6-trimethoxyphenyl)porphyrin; $H_2[T(2,4,6\text{-}Et)_3PP]$, *meso*-tetrakis(2,4,6-triethoxyphenyl)porphyrin; B, amine base; *N*-MeIm, *N*-methylimidazole; pip, piperidine.

0002-7863/82/1504-5992$01.25/0